Texture Alteration Detection in Bitemporal Images of Lesions with Psoriasis

Gabriela Maletti and Bjarne Ersbøll

Department of Informatics and Mathematical Modelling,
Technical University of Denmark,
DK-2800 Kgs. Lyngby, Denmark
{gmm, be}@imm.du.dk
http://www.imm.dtu.dk/image

Abstract. The objective of this work is to explore the feasibility of quantifying textural change between pairs of segmented patterns without registering them. The Multi-variate Alteration Detection (M.A.D.) Transform is applied to a texture model constructed with the data of segmented psoriasis lesions images. The texture model is Haralick's co-occurrence matrix, which is computed and normalized for each single band with the equalized data of a given lesion. The contribution of each single color band to the textural change is analyzed.

1 Introduction

We use a database consisting of a set of 175 images of lesions with psoriasis taken at the Gentofte Hospital of Denmark during four pilot sessions with three invited patients. For each patient, three lesions were captured five times during each session, along four weeks. The images were labelled with four characters, indicating patient (1, 2, 3), lesion (A, B, C), session (a, b, c, d) and capture (1, 2, 3, 4, 5) respectively. The original RGB images were reduced in size to $(576-20)/4$ rows by $(768-20)/4$ columns of pixels. The images can be assumed to contain three classes (background, normal skin and lesion), which were segmented with a two-stage hierarchical classification scheme [9]. This scheme separates, in the first stage, the skin from the background, and, in the second stage, the lesion from the normal skin. Since the images are affected by shadows, an illumination correction scheme was proposed [10].

To evaluate lesion changes between sessions, physicians make scores of a four-variables set: the redness, the scaling, the thickness and the body area covered by the lesions. Manual scoring highly depends on the dermatologist, who can show variations in criteria along sessions due to the huge amount of patients and lesions observed during each working day. In order to use a set of lesions like these as input to an automatic system that analyzes their change in time, it could be helpful to express the data in a way where they are comparable, without loosing connection with the original data. Registration of classified lesions patterns appear as options to possible solutions. However, they could have

a high computational cost.

To transform pairs of not registered original data to a space were the transformed data have a perfect registration is possible through a textural descriptor [17], [8], [13], [1], [7], [16], [15] that is invariant to translations and rotations of patterns, like Haralick's co-occurrence matrix [3]. On the other hand, a statistical approach that allows to detect alterations is the M.A.D. Transform (Multivariate Alteration Detection Transform) [11], [12]. This scheme transforms two sets of multi-variate observations into a difference between two linear combinations of the original variables explaining maximal change in all variables simultaneously.

The present work consists of the description of the following aspects: the textural model, the two-set canonical correlation analysis and the M.A.D. Transform. Results show the contribution of each color band to each M.A.D. component. Finally, a back-projection approach from the M.A.D. output to the original data is proposed.

2 The Texture Model

Following [6], let δ be a compact and convex set established in the image space as a circular window and let β be a vector position operator relating the relative spatial location of a pair of pixels in the window; for each single band, the co-occurrence matrix C is the estimated probability of having a pair of pixels (λ_p, λ_q) in the relative position given by β. The elements of the $Q \times Q$ co-occurrence matrix $C(\lambda_p, \lambda_q, \beta, \delta)$, with Q being the number of quantization levels, are given by:

$$\frac{O\{r|r, r+\beta \in \sigma(\delta), g(r) = \lambda_p, g(r+\beta) = \lambda_q\}}{O\{r|r+\beta \in \delta\}} \tag{1}$$

where $g(r)$ is the subset of the RGB image corresponding to the lesion with psoriasis, $\sigma(\delta)$ is a translation isometry over the window, O is the order of the set, and $r = (i, j)$ is the vector position of a pixel.

3 Two-Set Canonical Correlations Analysis

Conceptually, two-set canonical correlations analysis is a technique that finds corresponding sets of linear combinations -called canonical variables- of two groups of variables, such that the first canonical variables are the ones with the largest correlation, and higher order canonical variables are maximally correlated subject to orthogonality or uncorrelatedness with lower order canonical variables [11], [4].

Formally, let $\boldsymbol{x}_1$ and $\boldsymbol{x}_2$ be two sets of variables of dimensions m_1 and m_2 respectively, with $m_1 \leq m_2$. The two-set canonical correlation analysis chooses $m_1 + m_2$ linear transforms

$$\begin{array}{c} \boldsymbol{y}_{1i} = \boldsymbol{a}_{1i}^T \boldsymbol{x}_1, i = 1, ..., m_1 \\ \boldsymbol{y}_{2i} = \boldsymbol{a}_{2i}^T \boldsymbol{x}_2, i = 1, ..., m_2, \end{array} \tag{2}$$

such that the correlations within groups are

$$\begin{array}{c} Corr[\boldsymbol{a}_{1i}^T \boldsymbol{x}_1, \boldsymbol{a}_{1j}^T \boldsymbol{x}_1] = \delta_{ij} \\ Corr[\boldsymbol{a}_{2i}^T \boldsymbol{x}_2, \boldsymbol{a}_{2j}^T \boldsymbol{x}_2] = \delta_{ij} \end{array} \tag{3}$$

and the correlations between groups are

$$Corr[\boldsymbol{a}_{1i}^T \boldsymbol{x}_1, \boldsymbol{a}_{2j}^T \boldsymbol{x}_2] = \rho_j \delta_{ij} \tag{4}$$

where δ is the Kronecker delta.

Let the sets of variables $\boldsymbol{x}_1$ and $\boldsymbol{x}_2$ be described by the $m_1 + m_2$ dimensional variable

$$X = [\boldsymbol{x}_1^T \boldsymbol{x}_2^T] \tag{5}$$

and assume

$$E[\boldsymbol{X}] = 0 \wedge D[\boldsymbol{X}] = \Sigma = \begin{bmatrix} \Sigma_{11} & \Sigma_{12} \\ \Sigma_{21} & \Sigma_{22} \end{bmatrix} \tag{6}$$

with $\Sigma_{ij} \in \Re^{m_i x m_j}$ and

$$\Sigma_{ij} = \Sigma_{ji}^T, \forall i, j = 1, 2 \tag{7}$$

and non-singular.

We would like to find the transforms

$$\begin{array}{c} \boldsymbol{y}_1 = \boldsymbol{a}_1^T \boldsymbol{x}_1 \\ \boldsymbol{y}_2 = \boldsymbol{a}_2^T \boldsymbol{x}_2 \end{array} \tag{8}$$

with

$$D\{Y\} = \Sigma_Y = \begin{bmatrix} Var[\boldsymbol{y}_1] & Cov[\boldsymbol{y}_1, \boldsymbol{y}_2] \\ Cov[\boldsymbol{y}_2, \boldsymbol{y}_1] & Var[\boldsymbol{y}_1] \end{bmatrix} = \begin{bmatrix} \boldsymbol{a}_1^T \Sigma_{11} \boldsymbol{a}_1 & \boldsymbol{a}_1^T \Sigma_{12} \boldsymbol{a}_2 \\ \boldsymbol{a}_2^T \Sigma_{21} \boldsymbol{a}_1 & \boldsymbol{a}_2^T \Sigma_{22} \boldsymbol{a}_2 \end{bmatrix} \tag{9}$$

under the constraints

$$\begin{array}{c} Var[\boldsymbol{y}_1] = 1 \\ Var[\boldsymbol{y}_2] = 1 \end{array} \tag{10}$$

such that the correlation

$$\rho = Corr[\boldsymbol{y}_1, \boldsymbol{y}_2] = \frac{Cov[\boldsymbol{y}_1, \boldsymbol{y}_2]}{\sqrt{Var[\boldsymbol{y}_1] Var[\boldsymbol{y}_2]}} = \boldsymbol{a}_1^T \Sigma_{12} \boldsymbol{a}_2 \tag{11}$$

is maximized.

Let $\lambda_1/2$ and $\lambda_2/2$ be Lagrange multipliers introduced in

$$\psi = \boldsymbol{a}_1^T \Sigma_{12} \boldsymbol{a}_2 - \frac{\lambda_1}{2}(\boldsymbol{a}_1^T \Sigma_{11} \boldsymbol{a}_1 - 1) - \frac{\lambda_2}{2}(\boldsymbol{a}_2^T \Sigma_{22} \boldsymbol{a}_2 - 1). \tag{12}$$

We would like to maximize ψ with respect to $\boldsymbol{a}_1$ and $\boldsymbol{a}_2$. Due to the symmetry condition in Equation 7, the following matrix differentiation property can be applied

$$\frac{\partial(\boldsymbol{a}_i^T \Sigma_{ii} \boldsymbol{a}_i)}{\partial \boldsymbol{a}_i} = 2\Sigma_{ii}\boldsymbol{a}_i \tag{13}$$

and the partial derivatives of ψ with respect to $\boldsymbol{a}_1$ and $\boldsymbol{a}_2$ are

$$\frac{\partial \psi}{\partial \boldsymbol{a}_1} = \Sigma_{12}\boldsymbol{a}_2 - \lambda_1 \Sigma_{11}\boldsymbol{a}_1 \tag{14}$$

$$\frac{\partial \psi}{\partial \boldsymbol{a}_2} = \Sigma_{21}\boldsymbol{a}_1 - \lambda_2 \Sigma_{22}\boldsymbol{a}_2 \tag{15}$$

Note that Equations 14 and 15 could also be obtained by rewriting Equation 12 with λ_1 and λ_2 as dependent variables: λ_1 is derived with respect to $\boldsymbol{a}_1$ and λ_2, with respect to $\boldsymbol{a}_2$; the derivative of the quotient and the symmetry condition 7 is applied and the huge expressions obtained can easily be simplified because the main part of each one is only λ_1 and λ_2 respectively.

Setting the partial derivatives of ψ to zero and multiplying respectively by $\boldsymbol{a}_1^T$ and $\boldsymbol{a}_2^T$, we have

$$\boldsymbol{a}_1^T \Sigma_{12}\boldsymbol{a}_2 - \lambda_1 \boldsymbol{a}_1^T \Sigma_{11}\boldsymbol{a}_1 = 0 \tag{16}$$

$$\boldsymbol{a}_2^T \Sigma_{21}\boldsymbol{a}_1 - \lambda_2 \boldsymbol{a}_2^T \Sigma_{22}\boldsymbol{a}_2 = 0. \tag{17}$$

Due to $\boldsymbol{a}_1$ and $\boldsymbol{a}_2$ are scalars, the following property can be applied $\boldsymbol{a}_1^T \Sigma_{12}\boldsymbol{a}_2 = (\boldsymbol{a}_1^T \Sigma_{12}\boldsymbol{a}_2)^T$. The transpose of a product is the product of the transposes with inverted order, and using Equation 7, the correlation ρ between the transformed variables turns to be

$$\rho = \boldsymbol{a}_1^T \Sigma_{12}\boldsymbol{a}_2 = \boldsymbol{a}_2^T \Sigma_{21}\boldsymbol{a}_1 = \lambda_1 = \lambda_2 \tag{18}$$

Substituting Equation 18 in Equations 14 and 15

$$\Sigma_{12}\boldsymbol{a}_2 - \rho \Sigma_{11}\boldsymbol{a}_1 = 0 \tag{19}$$

$$\Sigma_{21}\boldsymbol{a}_1 - \rho \Sigma_{22}\boldsymbol{a}_2 = 0 \tag{20}$$

and multiplying Equation 20 by Σ_{22}^{-1} gives

$$\rho = \Sigma_{22}^{-1}\Sigma_{21}\frac{\boldsymbol{a}_1}{\boldsymbol{a}_2}. \tag{21}$$

Pre-multiplying Equation 19 with ρ, substituting it with Equation 21 and re-writing everything with respect to $\boldsymbol{a}_1$ we have

$$\Sigma_{12}\Sigma_{22}^{-1}\Sigma_{21}\boldsymbol{a}_1 = \rho^2\Sigma_{11}\boldsymbol{a}_1, \tag{22}$$

which is recognized as an eigenvalue problem. On the other hand, multiplying Equation 19 by Σ_{11}^{-1} gives

$$\rho = \Sigma_{11}^{-1}\Sigma_{12}\frac{\boldsymbol{a}_2}{\boldsymbol{a}_1}. \tag{23}$$

Substituting Equation 23 in - previously multiplied by the scalar ρ- Equation 20 we have

$$\Sigma_{21}\Sigma_{11}^{-1}\Sigma_{12}\boldsymbol{a}_2 = \rho^2\Sigma_{22}\boldsymbol{a}_2. \tag{24}$$

Rewriting Equations 22 and 24 we have the generalized equations of eigenvalues and eigenvectors:

$$[\Sigma_{11}^{-1}\Sigma_{12}\Sigma_{22}^{-1}\Sigma_{21} - \rho^2 I]\boldsymbol{a}_1 = 0 \tag{25}$$

and

$$[\Sigma_{22}^{-1}\Sigma_{21}\Sigma_{11}^{-1}\Sigma_{12} - \rho^2 I]\boldsymbol{a}_2 = 0. \tag{26}$$

The sets $\boldsymbol{y}_1$ and $\boldsymbol{y}_2$ are obtained by projecting the sets $\boldsymbol{x}_1$ and $\boldsymbol{x}_2$ onto the subspaces spanned by the eigenvectors $\boldsymbol{a}_1$ and $\boldsymbol{a}_2$ respectively with the corresponding largest eigenvalue equal to the square correlation.

If $m_1 = m_2$ the $\boldsymbol{y}_{1i}, i = 1, ..., m_1$ are obtained by projecting $\boldsymbol{x}_1$ onto the subspaces spanned by the eigenvectors $\boldsymbol{a}_{11}, ..., \boldsymbol{a}_{1m_1}$ corresponding to the eigenvalues $\rho_1^2 \geq ... \geq \rho_{m_1}^2$ of $\Sigma_{12}\Sigma_{22}^{-1}\Sigma_{21}$, and the $\boldsymbol{y}_{2i}, i = 1, ..., m_2$ are obtained by projecting $\boldsymbol{x}_2$ onto the subspaces spanned by the eigenvectors $\boldsymbol{a}_{21}, ..., \boldsymbol{a}_{2m_2}$ corresponding to the same eigenvalues. If $m_1 \leq m_2$ the eigenvalue problem in Equation 22 degenerates since the last eigenvalue will equal zero with $(m2 - m1)$ multiplicity.

4 The M.A.D. Transform

Again, for completeness, let us follow [11] for describing the M.A.D. Transform. Let X_1 and X_2 be two sets of variables of dimensions m_1 and m_2 respectively, with $m_1 \leq m_2$, $E\{\mathsf{X}_1\} = E\{\mathsf{X}_2\} = 0$ transformed with the coefficients from a standard canonical correlation analysis $\boldsymbol{a}_1$ and $\boldsymbol{a}_2$ in

$$\begin{array}{l} \mathsf{Y}_{1i} = \boldsymbol{a}_{1i}^T\mathsf{X}_1, i = 1, ..., m_1 \\ \mathsf{Y}_{2i} = \boldsymbol{a}_{2i}^T\mathsf{X}_2, i = 1, ..., m_2. \end{array} \tag{27}$$

Further, Y_1 and Y_2 are positively correlated and with unit variance, such that the variance of their difference is maximized.

$$Var[\boldsymbol{a}_1^T\mathsf{X}_1 - \boldsymbol{a}_2^T\mathsf{X}_2] = \tag{28}$$

$$Var[\boldsymbol{a}_1^T \boldsymbol{X}_1] + Var[\boldsymbol{a}_2^T \boldsymbol{X}_2] - 2Cov[\boldsymbol{a}_1^T \boldsymbol{X}_1, \boldsymbol{a}_2^T \boldsymbol{X}_2] \tag{29}$$

$$= 2(1 - Corr[\boldsymbol{a}_1^T \boldsymbol{X}_1, \boldsymbol{a}_2^T \boldsymbol{X}_2]) \tag{30}$$

The M.A.D. Transform consists of the variates obtained when the corresponding canonical variates are subtracted in reverse order, what means that the m_1^{th} difference shows maximum variance among such variables, and the $(m_1 - j)^{th}$ difference shows maximum variance subject to the constraint that this difference is not correlated with the previous j ones. The M.A.D. variates are invariant to linear and affine scaling, what is not the case of the Principal Components. The dispersion matrix of the M.A.D. variates is

$$D[\boldsymbol{a}_1^T \boldsymbol{X}_1 - \boldsymbol{a}_2^T \boldsymbol{X}_2] = 2(\boldsymbol{I} - \boldsymbol{R}) \tag{31}$$

where $\boldsymbol{I}$ is the $m_1 \times m_1$ unit matrix and $\boldsymbol{R}$ is the $m_1 \times m_1$ matrix containing the sorted canonical correlations on the diagonal and zeros off the diagonal.

5 Results and Discussion

In order to evaluate the color band contribution in the textural change of the lesions, the following experiment was designed. The set of 175 captures obtained at Gentofte's Hospital allowed the construction of 650 pairs of captures with the same time increment of one week between them. For each image of a given patient and lesion, each one of the five images of the next session were associated. For each one of the 175 images, the histogram of the pixels belonging to the area of the thematic map indicating a lesion was first equalized. For each single image, a three band synthetical image of 256 by 256 pixels was constructed in the following way: for each single band, the co-occurrence matrix of the region indicating the single lesion included was constructed and normalized.

Two sets of 650 pairs of images were used to apply the present scheme: the first set was given by the original images; the second set, by the illumination-corrected images (see Figures 13 to 21 in [10]). For each single image, the co-occurrence matrix of the equalized region indicating skin was generated. For each pair of original and illumination-corrected images of the same capture, the same thematic map indicating skin was used (See Figures 2 to 8 in [9]). In order to reduce the influence of very high values, logarithms were applied to the normalized co-occurrence matrix values:

$$y[r, c, b] = \frac{x[r, c, b]}{\sum_r \sum_c x[r, c, b]}. \tag{32}$$

After that, the values were again normalized:

$$z[r, c, b] = \frac{(log(y[r, c, b] * map[r, c, 1] + (1 - map[r, c, b])) + \beta[b]) * map[r, c]}{\sum_{k,l}(z[k, l, b] * map[k, l, b])} \tag{33}$$

where $map[r,c,b]$ is 1 if $y[r,c,b] > 0$ and 0, otherwise, and

$$\beta[b] = max(|z[r,c,b]|) \tag{34}$$

$\forall r, c$.

The matrix is now an image. For each pair of synthetical images constructed in the way mentioned, the M.A.D. transform was applied. For this stage, it was helpful to use the following programs: *fhist* [2], *gclm* [2] [14] and *maf* [5]. For each pair of images of the data-set, the union of the maps indicating positive values for each co-occurrence matrix was generated; the M.A.D. Transform was only applied to the pixels included in that map. Tables 1 and 2 show the results obtained for the sets of original images. Tables 3 and 4 show the results obtained for the sets of illumination-corrected images[1].

Each single cell value in Tables 1 and 3 is the average absolute correlation value between the normalized co-occurrence matrix of the $b-th$ color bands and the $m-th$ MAD components of all pairs of images of the $l-th$ lesion of the $p-th$ patient. It is computed in the following way:

$$E[\rho_{p,l,b,m}] = \frac{1}{(n_s - \delta t)n_c^2} \sum_{s=1}^{n_s-\delta t} \sum_{i=1}^{n_c} \sum_{j=1}^{n_c} a_{p,l,s,i,\delta_t,j,b,m} \tag{35}$$

where

$$a_{p,l,s,i,\delta_t,j,b,m} = \frac{1}{2}(|\rho[X_{p,l,s,i,b}, MAD_{p,l,s,i,\delta t,j,b}, m]| + |\rho[X_{p,l,s+\delta t,j,b}, MAD_{p,l,s,i,\delta t,j,b}, m]|) \tag{36}$$

and ρ is the correlation coefficient, δt is the time increment (in this case, δt is one week). The indexes i and j indicate the capture number within a session. $MAD_{p,l,s,i,\delta t,j,b,m}$ equals to $MAD[X_{p,l,s,i,b}, X_{p,l,s+\delta t,j,b}, m]$.

Each single cell value in Tables 2 and 4 is the standard deviation of the averaged absolute correlation values between the normalized co-occurrence matrix of the $b-th$ color bands and the $m-th$ MAD components of all pairs of images of the $l-th$ lesion of the $p-th$ patient. It is computed in the following way:

$$S[\rho_{p,l,b,m}] = \sqrt{\frac{1}{(n_s - \delta t)n_c^2} \sum_{s=1}^{n_s-\delta t} \sum_{i=1}^{n_c} \sum_{j=1}^{n_c} (a^2_{p,l,s,i,\delta_t,j,b,m}) - E[\rho_{p,l,b,m}]^2} \tag{37}$$

where the symbols have the same meaning as before.

[1] The original HIPS formatted images were used in combination with the TIFF formatted illumination function to produce the illumination-corrected images in HIPS format. These images were equalized and then the co-occurrence matrix was computed.

Table 1. Average Absolute Correlation Values per Lesion of *RGB* skin data with their respective M.A.D. Components

(Patient,Lesion)	(R,MAD1)	(G,MAD1)	(B,MAD1)
(1,A)	0.163069	0.181529	0.052689
(1,B)	0.093642	0.216019	0.109057
(1,C)	0.150723	0.199478	0.137738
(2,A)	0.117731	0.151841	0.187481
(2,B)	0.094710	0.230283	0.130987
(2,C)	0.111509	0.133244	0.182223
(3,A)	0.038838	0.195560	0.163730
(3,B)	0.032641	0.206640	0.203355
(3,C)	0.043867	0.228722	0.198393
(Patient,Lesion)	(R,MAD2)	(G,MAD2)	(B,MAD2)
(1,A)	0.149579	0.083112	0.188200
(1,B)	0.236058	0.085506	0.155400
(1,C)	0.261095	0.131136	0.178398
(2,A)	0.238930	0.149425	0.080667
(2,B)	0.247828	0.052757	0.160879
(2,C)	0.233855	0.098236	0.082241
(3,A)	0.252858	0.062821	0.119769
(3,B)	0.280739	0.109337	0.099062
(3,C)	0.285794	0.086110	0.127319
(Patient,Lesion)	(R,MAD3)	(G,MAD3)	(B,MAD3)
(1,A)	0.167162	0.170654	0.168428
(1,B)	0.184625	0.193093	0.195325
(1,C)	0.226380	0.242602	0.240919
(2,A)	0.244500	0.255134	0.260686
(2,B)	0.192198	0.197892	0.200079
(2,C)	0.279305	0.296285	0.289731
(3,A)	0.165526	0.181658	0.180395
(3,B)	0.204145	0.216882	0.217735
(3,C)	0.192946	0.202501	0.202845

Table 2. Standard Deviation of the Absolute Correlation Values per Lesion of the *RGB* skin data with the M.A.D. Components

(Patient,Lesion)	(R,MAD1)	(G,MAD1)	(B,MAD1)
(1,A)	0.025971	0.016633	0.030963
(1,B)	0.028369	0.019309	0.026687
(1,C)	0.031737	0.014496	0.019820
(2,A)	0.059834	0.030295	0.014737
(2,B)	0.040232	0.010890	0.029503
(2,C)	0.070107	0.042084	0.076832
(3,A)	0.012120	0.010609	0.013386
(3,B)	0.017749	0.009709	0.013645
(3,C)	0.029494	0.014647	0.023083
(Patient,Lesion)	(R,MAD2)	(G,MAD2)	(B,MAD2)
(1,A)	0.028772	0.023656	0.017764
(1,B)	0.026801	0.043394	0.016797
(1,C)	0.022621	0.023489	0.020474
(2,A)	0.033550	0.029944	0.027297
(2,B)	0.018773	0.023604	0.023727
(2,C)	0.059343	0.032142	0.047481
(3,A)	0.011745	0.019359	0.008171
(3,B)	0.017558	0.016535	0.030054
(3,C)	0.022625	0.032087	0.036531
(Patient,Lesion)	(R,MAD3)	(G,MAD3)	(B,MAD3)
(1,A)	0.013872	0.012831	0.012198
(1,B)	0.024374	0.025512	0.028243
(1,C)	0.011900	0.014789	0.014719
(2,A)	0.031265	0.031427	0.034579
(2,B)	0.014287	0.013550	0.014184
(2,C)	0.038647	0.043020	0.036207
(3,A)	0.021784	0.021555	0.022279
(3,B)	0.021174	0.023636	0.023704
(3,C)	0.012659	0.014226	0.016471

Table 3. Average Absolute Correlation Values per Lesion of the illumination-corrected *RGB* skin data with their respective M.A.D. Components

(Patient,Lesion)	(R,MAD1)	(G,MAD1)	(B,MAD1)
(1,A)	0.170079	0.176821	0.073168
(1,B)	0.183584	0.193015	0.093375
(1,C)	0.208084	0.204445	0.076428
(2,A)	0.099910	0.214296	0.151165
(2,B)	0.150016	0.196696	0.171897
(2,C)	0.070576	0.187925	0.195604
(3,A)	0.113855	0.222418	0.142154
(3,B)	0.024691	0.208501	0.202745
(3,C)	0.090282	0.221817	0.190266
(Patient,Lesion)	(R,MAD2)	(G,MAD2)	(B,MAD2)
(1,A)	0.154035	0.074054	0.201950
(1,B)	0.203793	0.137015	0.198929
(1,C)	0.186940	0.094268	0.245279
(2,A)	0.249320	0.059774	0.159474
(2,B)	0.229558	0.132791	0.145819
(2,C)	0.282807	0.088674	0.073255
(3,A)	0.255834	0.040157	0.182085
(3,B)	0.276600	0.100579	0.105682
(3,C)	0.285825	0.080852	0.142917
(Patient,Lesion)	(R,MAD3)	(G,MAD3)	(B,MAD3)
(1,A)	0.177938	0.183928	0.178287
(1,B)	0.214027	0.220947	0.222161
(1,C)	0.200914	0.208052	0.203250
(2,A)	0.181045	0.188425	0.187791
(2,B)	0.202083	0.209892	0.211410
(2,C)	0.220413	0.235589	0.234932
(3,A)	0.179750	0.188971	0.186960
(3,B)	0.208101	0.217542	0.217578
(3,C)	0.198283	0.208827	0.208337

Table 4. Standard Deviation of the Absolute Correlation Values per Lesion of the illumination-corrected RGB skin data with the M.A.D. Components

(Patient,Lesion)	(R,MAD1)	(G,MAD1)	(B,MAD1)
(1,A)	0.039767	0.018222	0.036756
(1,B)	0.043357	0.034397	0.047152
(1,C)	0.017927	0.021666	0.017569
(2,A)	0.032620	0.019728	0.024057
(2,B)	0.088681	0.040340	0.058499
(2,C)	0.045544	0.024256	0.043097
(3,A)	0.027636	0.008405	0.017570
(3,B)	0.021223	0.014558	0.014621
(3,C)	0.033461	0.023677	0.024106
(Patient,Lesion)	(R,MAD2)	(G,MAD2)	(B,MAD2)
(1,A)	0.045084	0.031534	0.017648
(1,B)	0.045152	0.059842	0.043288
(1,C)	0.024923	0.029271	0.006875
(2,A)	0.023577	0.043846	0.027413
(2,B)	0.075262	0.052789	0.051839
(2,C)	0.033527	0.032352	0.030808
(3,A)	0.017790	0.018396	0.011767
(3,B)	0.018079	0.021996	0.018503
(3,C)	0.021804	0.046565	0.038868
(Patient,Lesion)	(R,MAD3)	(G,MAD3)	(B,MAD3)
(1,A)	0.014500	0.015754	0.014663
(1,B)	0.028974	0.029582	0.035410
(1,C)	0.006570	0.005675	0.006290
(2,A)	0.009182	0.010115	0.010683
(2,B)	0.009957	0.011238	0.011484
(2,C)	0.020532	0.024252	0.025135
(3,A)	0.007396	0.007803	0.009210
(3,B)	0.030657	0.033255	0.033002
(3,C)	0.015375	0.017395	0.019219

Looking at the upper part of Table 1, it seems that for some cases, most of the contribution in the textural change is given by the red and the green bands (cases $(1, A)$ and $(1, C)$), and in others, by the green and the blue bands (the remaining cases). On the other hand, after illumination correction, the values reported in Table 3 indicate that for all the cases of the patient 1, most of the contribution in the textural change is given by the red and the green band and, for instance, the contribution of the red band in the textural change of the case $(3, A)$ is quite significant.

There is an aspect that was not taken into account during the design of the experiment. This was the lesion to skin ratio. As was mentioned in Section 2.1 of [9], the size between lesions [2] has a significant variance. In other words, the proportion of the area covered by the lesion with respect to the area covered by the skin is quite variable. On the other hand, there are cases for which the skin is completely covered by very small lesions, such that the whole classified region indicating skin could be considered part of the class lesion, and the second stage of the classification scheme, is not necessary. This means, that it may be necessary to redesign the experiment in order to compare more homogeneous data.

The same procedure as before was repeated for the cases $(1, A)$, $(1, B)$, $(1, C)$ and $(2, B)$, now using thematic maps indicating lesions. This means, that the normal skin was excluded. For patient 1, the thematic maps indicating lesions generated after illumination correction of the original images were used (see Figures 22 (case $(1, A)$), 23 (case $(1, B)$) and 24 (case $(1, c)$) in [10]). The objects were selected using an automated algorithm developed that assumes that the object of largest size in the thematic map is the desired lesion. The outputs are presented in Section A. For patient 2, the thematic maps used were produced with user-interaction assuming circular shape of the lesion. The user was required to provide for each single image, one single point, which was assumed to be the lesion center. A radius of that circle was also required. It was assumed that for a given lesion, all the shapes had the same radius. This was done for the lesion B (see Figure in Section A). Lesion C was excluded because it is partically covered by hair and the manual selection of one small homogeneous region turns to be difficult. For patient 3, the procedure was not applied, because it can be considered that the whole region indicating skin, is covered by lesion.

As illustration examples, some co-occurrence matrixes computed with data of illumination corrected images are shown in Appendix B. For the cases $(1, A)$, $(1, B)$, $(1, C)$ and $(2, B)$, the co-occurrence matrixes were computed using the data indicated in Appendix A. To compute the co-occurrence matrixes of the cases $(2, C)$, $(3, B)$ and $(3, C)$ the corresponding data sets used can be seen in Figures 6 to 8 of [9] respectively. For the cases $(2, A)$ and $(3, A)$ an artificial map for the down-sampled version of the original images was generated, indicating

[2] This means the size between the lesions of the different cases: $(1, A)$, $(1, B)$, $(1, C)$, $(2, A)$, $(2, B)$, $(2, C)$, $(3, A)$, $(3, B)$ and $(3, C)$.

Table 5. Average Absolute Correlation Values per Lesion of *RGB* lesion data with their respective M.A.D. Components

(Patient,Lesion)	(R,MAD1)	(G,MAD1)	(B,MAD1)
(1,A)	0.228414	0.241037	0.249670
(1,B)	0.087517	0.291845	0.257182
(1,C)	0.021994	0.444337	0.468673
(2,B)	0.021226	0.524634	0.387158
(Patient,Lesion)	(R,MAD2)	(G,MAD2)	(B,MAD2)
(1,A)	0.299963	0.154635	0.242142
(1,B)	0.334106	0.108684	0.195718
(1,C)	0.101731	0.469909	0.454413
(2,B)	0.061194	0.400099	0.518758
(Patient,Lesion)	(R,MAD3)	(G,MAD3)	(B,MAD3)
(1,A)	0.268627	0.300383	0.275886
(1,B)	0.270752	0.272509	0.266351
(1,C)	0.449892	0.046755	0.039726
(2,B)	0.399107	0.017429	0.019905

Table 6. Standard Deviation of the Absolute Correlation Values per Lesion of the *RGB* lesion data with the M.A.D. Components

(Patient,Lesion)	(R,MAD1)	(G,MAD1)	(B,MAD1)
(1,A)	0.075189	0.051723	0.120361
(1,B)	0.050564	0.057280	0.092927
(1,C)	0.010095	0.050346	0.045895
(2,B)	0.012165	0.078557	0.100383
(Patient,Lesion)	(R,MAD2)	(G,MAD2)	(B,MAD2)
(1,A)	0.068989	0.070599	0.110723
(1,B)	0.091141	0.094951	0.078275
(1,C)	0.022922	0.034339	0.042043
(2,B)	0.014210	0.087458	0.069111
(Patient,Lesion)	(R,MAD3)	(G,MAD3)	(B,MAD3)
(1,A)	0.015704	0.025307	0.022419
(1,B)	0.077885	0.095661	0.094163
(1,C)	0.024233	0.025523	0.019999
(2,B)	0.014610	0.009277	0.008870

Table 7. Average Absolute Correlation Values per Lesion of the illumination-corrected *RGB* lesion data with their respective M.A.D. Components

(Patient,Lesion)	(R,MAD1)	(G,MAD1)	(B,MAD1)
(1,A)	0.156864	0.251143	0.306729
(1,B)	0.134858	0.280693	0.287114
(1,C)	0.020100	0.438892	0.477563
(2,B)	0.024732	0.531542	0.375503
(Patient,Lesion)	(R,MAD2)	(G,MAD2)	(B,MAD2)
(1,A)	0.356152	0.151465	0.151860
(1,B)	0.326464	0.178192	0.196218
(1,C)	0.103229	0.475666	0.448373
(2,B)	0.064307	0.391578	0.524883
(Patient,Lesion)	(R,MAD3)	(G,MAD3)	(B,MAD3)
(1,A)	0.263711	0.298394	0.279176
(1,B)	0.292042	0.290461	0.282628
(1,C)	0.449129	0.048744	0.041427
(2,B)	0.400400	0.015945	0.019321

Table 8. Standard Deviation of the Absolute Correlation Values per Lesion of the illumination-corrected *RGB* lesion data with the M.A.D. Components

(Patient,Lesion)	(R,MAD1)	(G,MAD1)	(B,MAD1)
(1,A)	0.073514	0.043622	0.104251
(1,B)	0.084878	0.075100	0.108610
(1,C)	0.012400	0.049313	0.043281
(2,B)	0.011909	0.085662	0.100957
(Patient,Lesion)	(R,MAD2)	(G,MAD2)	(B,MAD2)
(1,A)	0.069711	0.055424	0.111003
(1,B)	0.094358	0.099449	0.092184
(1,C)	0.022383	0.033330	0.039751
(2,B)	0.017439	0.090638	0.071341
(Patient,Lesion)	(R,MAD3)	(G,MAD3)	(B,MAD3)
(1,A)	0.013473	0.022410	0.021080
(1,B)	0.068711	0.085562	0.081845
(1,C)	0.022226	0.023979	0.019838
(2,B)	0.013120	0.008677	0.009668

the whole image as being lesion. The contribution of each single color band to the first M.A.D. component of these examples can be seen in Table 9.

According to the added results (see upper part of Tables 5 and 7), it is surprising to see that while in the medical area the redness is the variable used for measuring change in lesions with psoriasis, it is mostly the green if not the blue band which contributes most significantly to the first M.A.D. component. These results have to be interpreted with caution, because of the small size of the data-set used.

6 Back-projection to the original data

To back-project the output of previous Section to the original data the following aspects have to be taken into account:

- For each pixel in the image and for each single band value, co-occurrences were computed with neighbors in eight directions. The output of the M.A.D. Transform is referred to these directions. There is not a one-to-one correspondence that allows to back-project the output of the M.A.D. Transform to the original data. Therefore, some constraints have to be set.
- The M.A.D. Transform is a difference of canonical variables, which come from an eigen-decomposition. Eigenvectors give a direction, but not a sense. The constraint for the M.A.D. Transform is that the eigenvectors are chosen so that the correlation between the canonical variables is positive ([11], page 85). However, an aspect not considered here, but that could be explored further, is if there are real cases for which the a negative correlation between canonical variables could be more interesting to analyze; for instance, a region that in a given time is normal and in a next time is ill, and viceversa.
- Again, the M.A.D. Transform is a difference of canonical variables. For the case of the co-occurrence matrix, each one of these variables are a new co-occurrence matrix corresponding to a new (unknown) texture.

To back-project the data from the M.A.D. Transform to the original images, the following criterion was applied. As it was mentioned, the M.A.D. components are computed with the co-occurrence matrix of each single band of two equalized images. For each pixel in each equalized image, co-occurrence pairs in eight directions were formed for each single band value. Each pair is used as index in a weighting function given by the absolute value of the first M.A.D. component. This was done, because only the magnitude of the change was considered of interest. For a given pixel, the M.A.D. absolute values corresponding to each co-occurrence pair formed by the pixel with its neighbors pixel in 8-connectivity [3], are summed and saved in a synthetical image. The histogram of this image is finally divided in two parts by a user set threshold. The segmentation output

[3] 3 bands by 8 pairs gives 24 weights

obtained is composed by a region indicating more textural change and region indicating less textural change.

The output of the back-projection scheme proposed is shown for two examples: the lesions $(1, A)$ and $(1, B)$. In both cases, the illumination corrected images with the lesion region equalized were used. The output of the M.A.D. Transform was back-projected to the original data in the way previously described. Note in each case that for each image of the pair, the segmented regions showing more and less textural change are approximately corresponding. This gives the evidence that it is possible to avoid the alignment and registration of images applying the M.A.D. transform to multi-spectral descriptors that are invariant to rotations and translations.

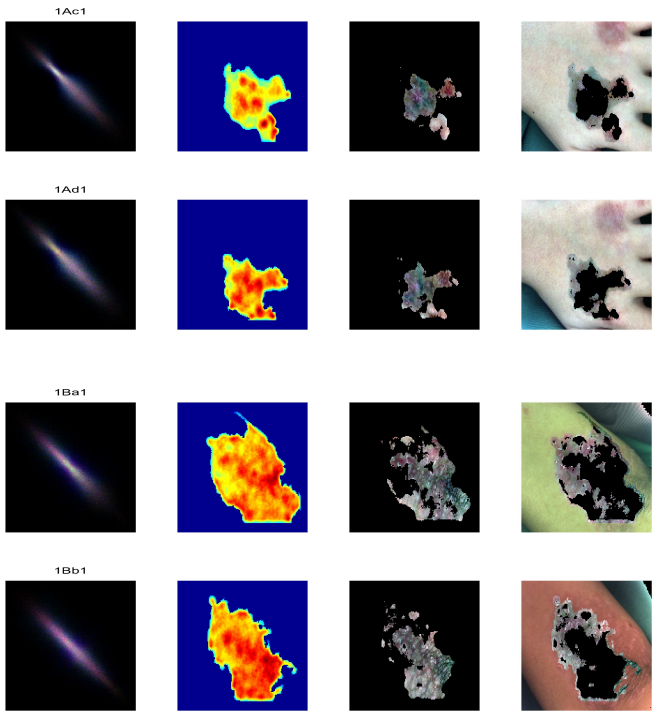

Fig. 1. From the M.A.D. Transform to the Original Data.
From left to right: co-occurrence matrix, back-projection synthetical map, regions with more textural change and regions with less textural change. From top to bottom: the first two rows are data for the case $(1, A)$ (the first images of the third and fourth session) and the last two rows, for the case $(1, B)$ (the first images of the first and second session).

However, it has to said that, in general, the output of the back-projection approach was not satisfactory. Each step and constraints set for the back-projection should be revised. The first M.A.D. component is the difference of canonical variables of the co-occurrence matrixes, that, in fact, correspond to a new textural version of the original images. For the back-projection, a combination of the original data and the first M.A.D. component was used, what could have been an unappropriate mixture of information. As it was mentioned in [12], the simple difference of the spectral bands, turns to be difficult to show the change in all the bands simultaneously. Thus, may be, for simplicity, in order to obtain a more suitable back-projection scheme, to start with a single difference of one pair of co-occurrence matrixes could be more a more fortunate way to follow.

7 Conclusions

The application of the Multi-variate Alteration Detection Transform to the normalized co-occurrence matrix of lesions with psoriasis patterns is a suitable approach for detecting texture changes in time that avoids the interaction with the user and the lesion pattern registration. The most significant contribution in the texture change of lesions with psoriasis is given -for the pilot data-set- by the green and blue bands. There is evidence that it is possible to back-project the M.A.D. Transform output to the original data, such that corresponding regions showing more and less textural change can be delineated. However, in order to be able to generalize the approach, the optimization of each single stage of the whole procedure has to be considered.

Acknowledgments

To the SITE Project funded by a grant from the Danish Technical Research Foundation (Project Number *STVF* 56-00-0123) for supporting the present work. To the dermatologists Lone Skov and Bo Bang of the Gentofte Hospital of Denmark and to the anonymous patients, for their collaboration during the image acquisition sessions.

Appendix

A Selected Lesions

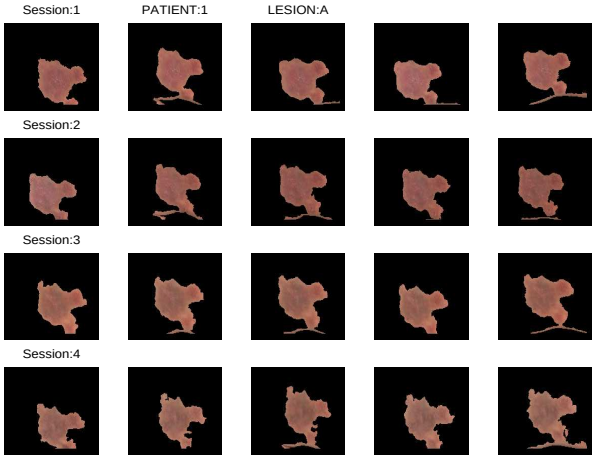

Fig. 2. Regions indicating the selected lesion A of patient 1 in the illumination-corrected images.

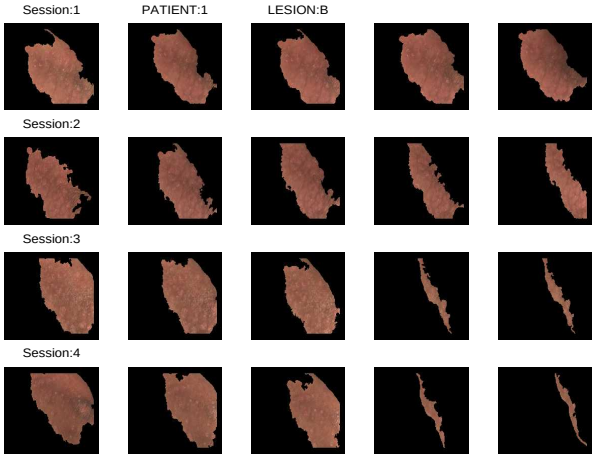

Fig. 3. Regions indicating the selected lesion B of patient 1 in the illumination-corrected images.

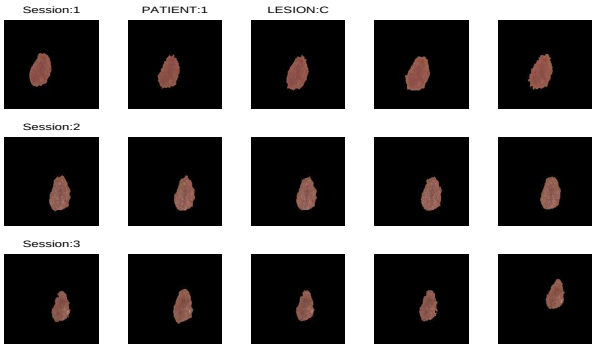

Fig. 4. Regions indicating the selected lesion C of patient 1 in the illumination-corrected images.

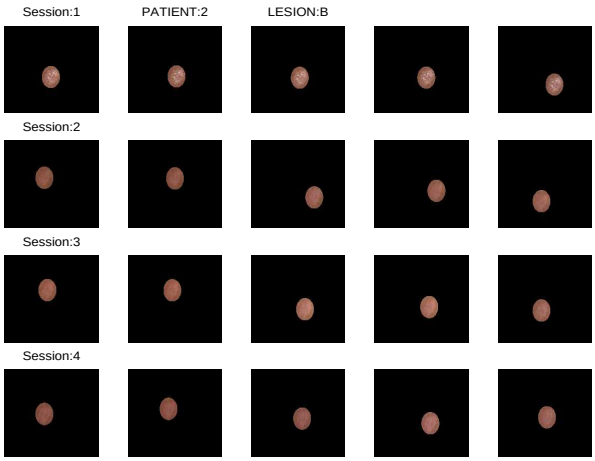

Fig. 5. Regions indicating the selected lesion B of patient 2 in the illumination-corrected images.

B Co-occurrence matrix of selected pairs of images and their MAD Transform

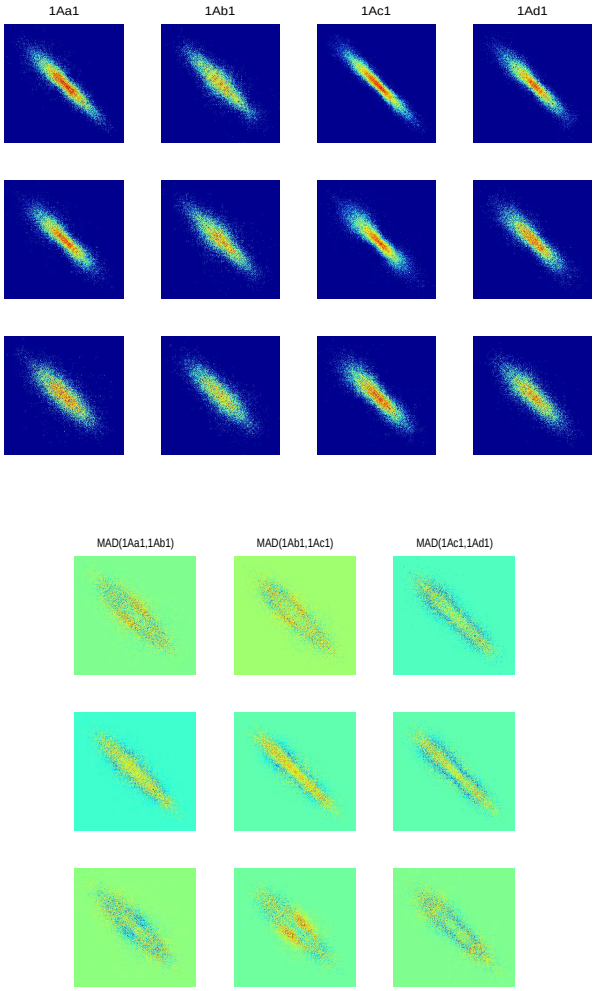

Fig. 6. Co-occurrence matrixes and M.A.D. Components for the case $(1, A)$. The upper part shows the co-occurrence matrixes of the lesion region of selected illumination-corrected images of (Patient 1, Lesion A); from top to bottom, the rows correspond to the red, green and blue band respectively. The lower part shows the MAD components of pairs of consecutive co-occurrence matrixes; from top to bottom, the row number is associated with the MAD component number.

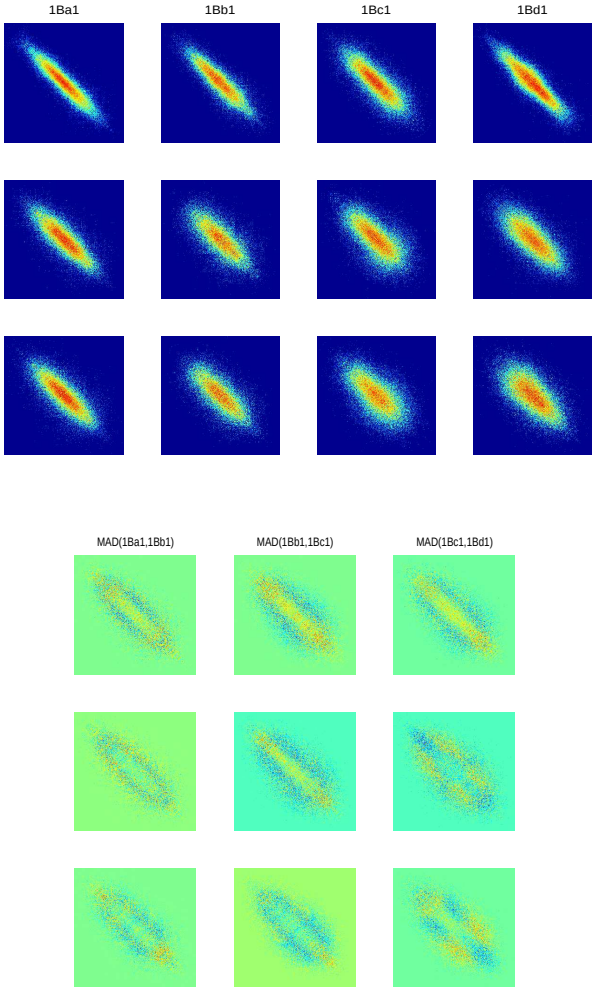

Fig. 7. Co-occurrence matrixes and M.A.D. Components for the case $(1, B)$.
The upper part shows the co-occurrence matrixes of the lesion region of selected illumination-corrected images of (Patient 1, Lesion B); from top to bottom, the rows correspond to the red, green and blue band respectively. The lower part shows the MAD components of pairs of consecutive co-occurrence matrixes; from top to bottom, the row number is associated with the MAD component number.

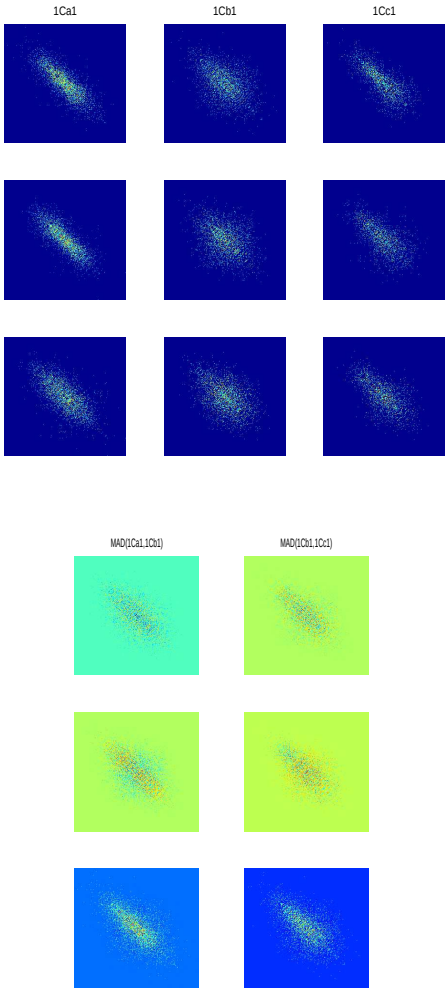

Fig. 8. Co-occurrence matrixes and M.A.D. Components for the case $(1, C)$. The upper part shows the co-occurrence matrixes of the lesion region of selected illumination-corrected images of (Patient 1, Lesion C); from top to bottom, the rows correspond to the red, green and blue band respectively. The lower part shows the MAD components of pairs of consecutive co-occurrence matrixes; from top to bottom, the row number is associated with the MAD component number.

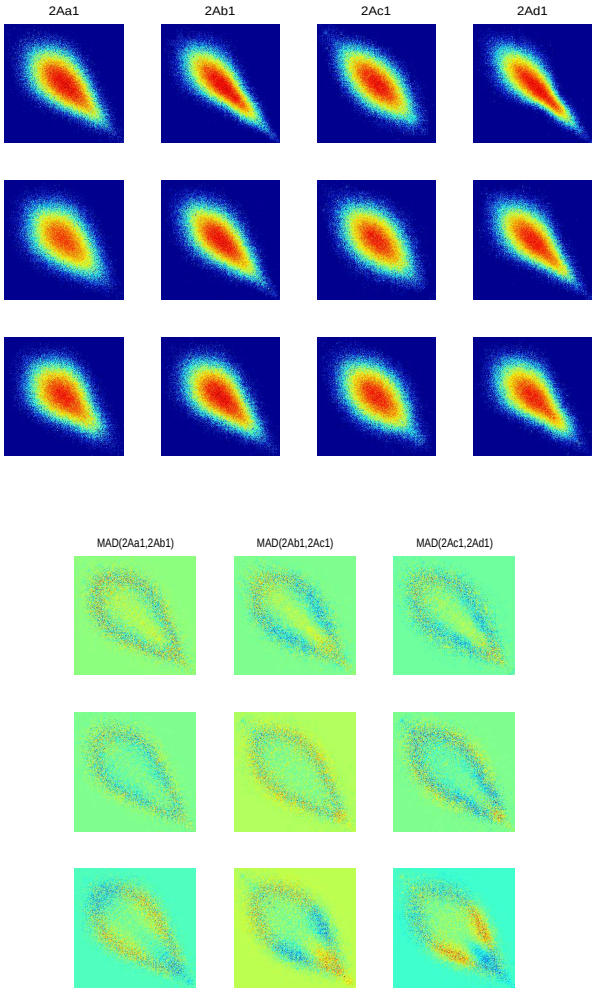

Fig. 9. Co-occurrence matrixes and M.A.D. Components for the case $(2, A)$. The upper part shows the co-occurrence matrixes of the lesion region of selected illumination-corrected images of (Patient 2, Lesion A); from top to bottom, the rows correspond to the red, green and blue band respectively. The lower part shows the MAD components of pairs of consecutive co-occurrence matrixes; from top to bottom, the row number is associated with the MAD component number.

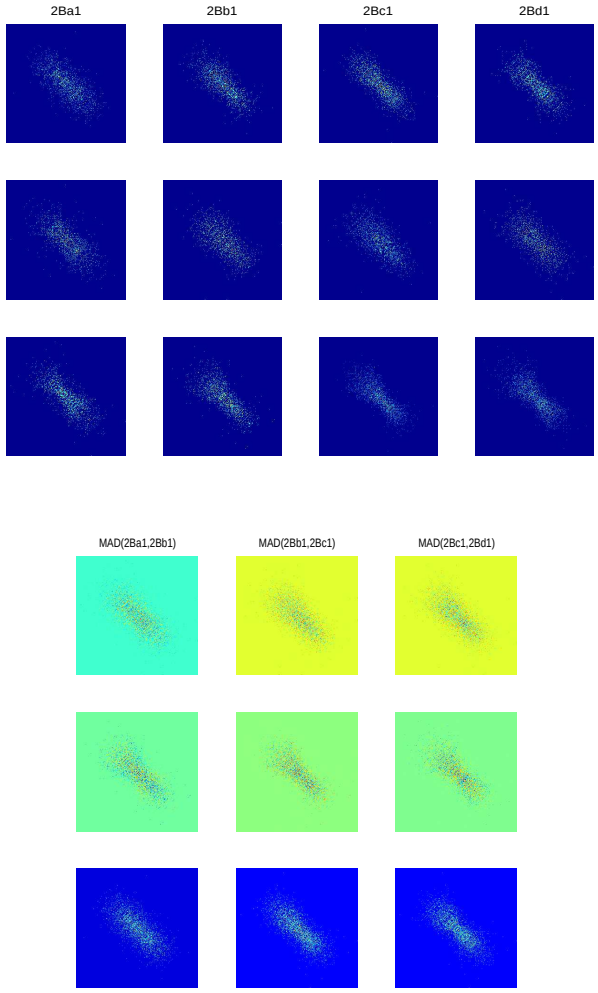

Fig. 10. Co-occurrence matrixes and M.A.D. Components for the case $(2, B)$. The upper part shows the co-occurrence matrixes of the lesion region of selected illumination-corrected images of (Patient 2, Lesion B); from top to bottom, the rows correspond to the red, green and blue band respectively. The lower part shows the MAD components of pairs of consecutive co-occurrence matrixes; from top to bottom, the row number is associated with the MAD component number.

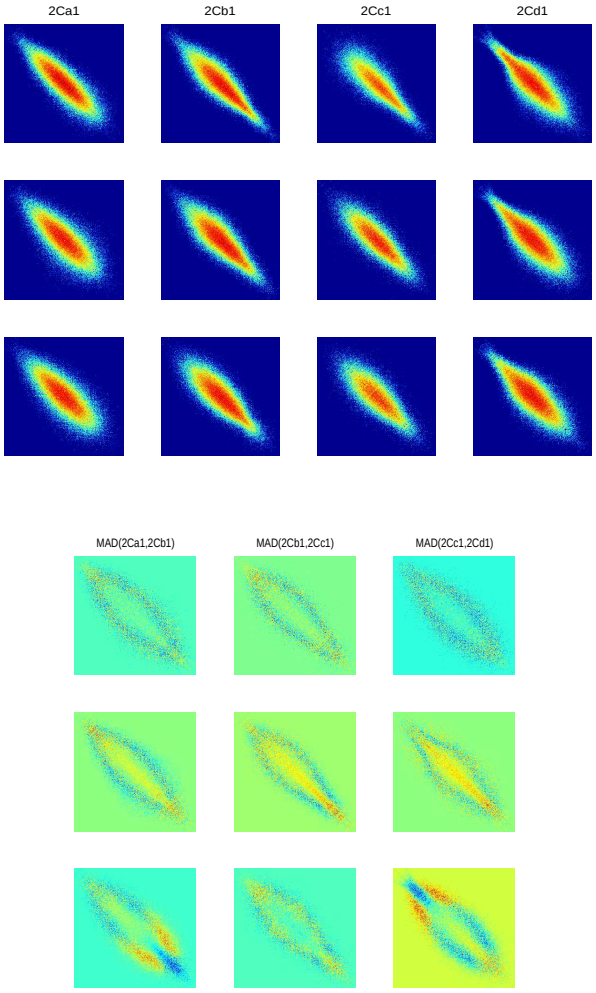

Fig. 11. Co-occurrence matrixes and M.A.D. Components for the case $(2, C)$. The upper part shows the co-occurrence matrixes of the lesion region of selected illumination-corrected images of (Patient 2, Lesion C); from top to bottom, the rows correspond to the red, green and blue band respectively. The lower part shows the MAD components of pairs of consecutive co-occurrence matrixes; from top to bottom, the row number is associated with the MAD component number.

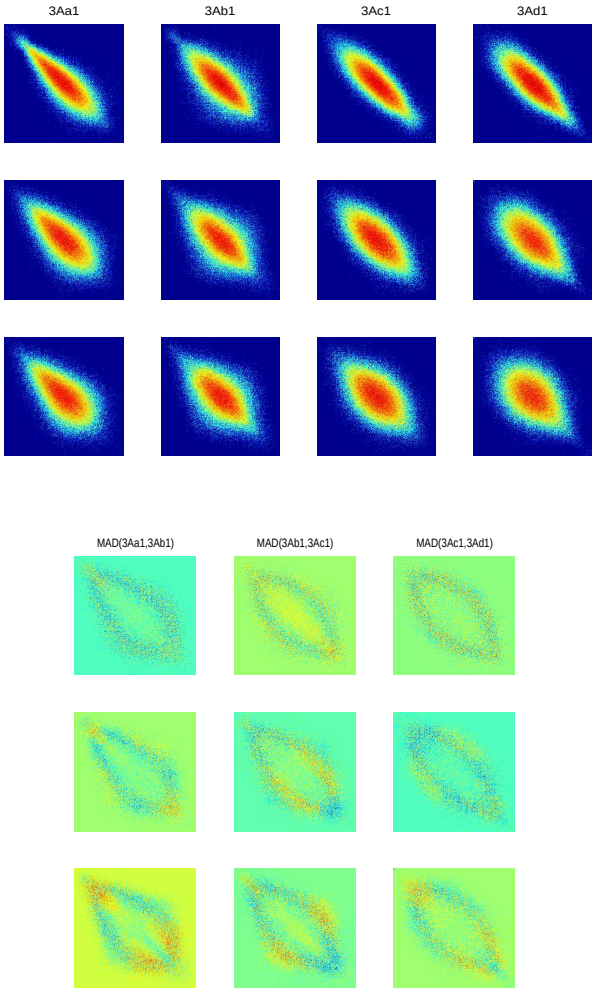

Fig. 12. Co-occurrence matrixes and M.A.D. Components for the case $(3, A)$. The upper part shows the co-occurrence matrixes of the lesion region of selected illumination-corrected images of (Patient 3, Lesion A); from top to bottom, the rows correspond to the red, green and blue band respectively. The lower part shows the MAD components of pairs of consecutive co-occurrence matrixes; from top to bottom, the row number is associated with the MAD component number.

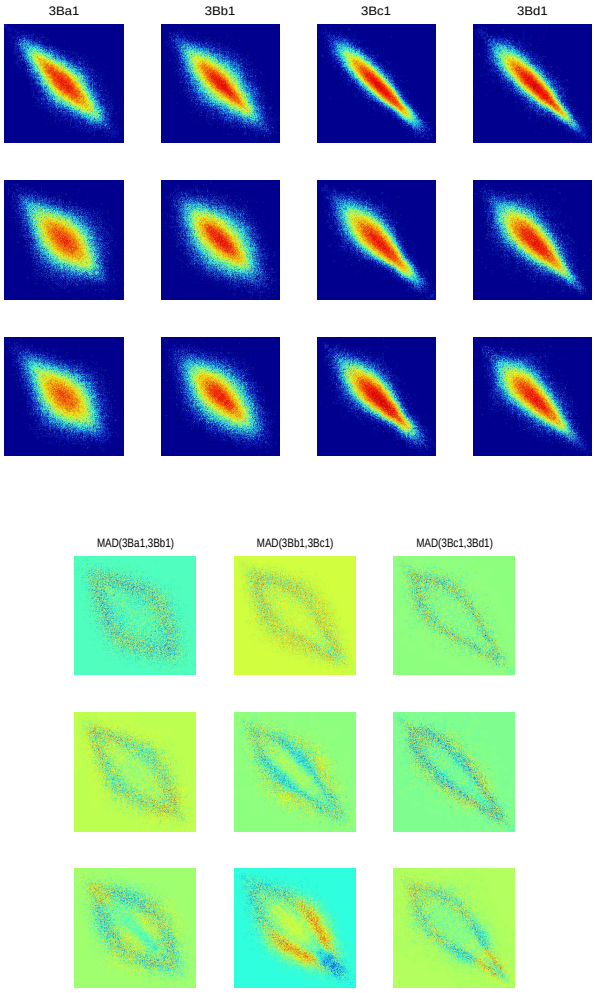

Fig. 13. Co-occurrence matrixes and M.A.D. Components for the case $(3, B)$. The upper part shows the co-occurrence matrixes of the lesion region of selected illumination-corrected images of (Patient 3, Lesion B); from top to bottom, the rows correspond to the red, green and blue band respectively. The lower part shows the MAD components of pairs of consecutive co-occurrence matrixes; from top to bottom, the row number is associated with the MAD component number.

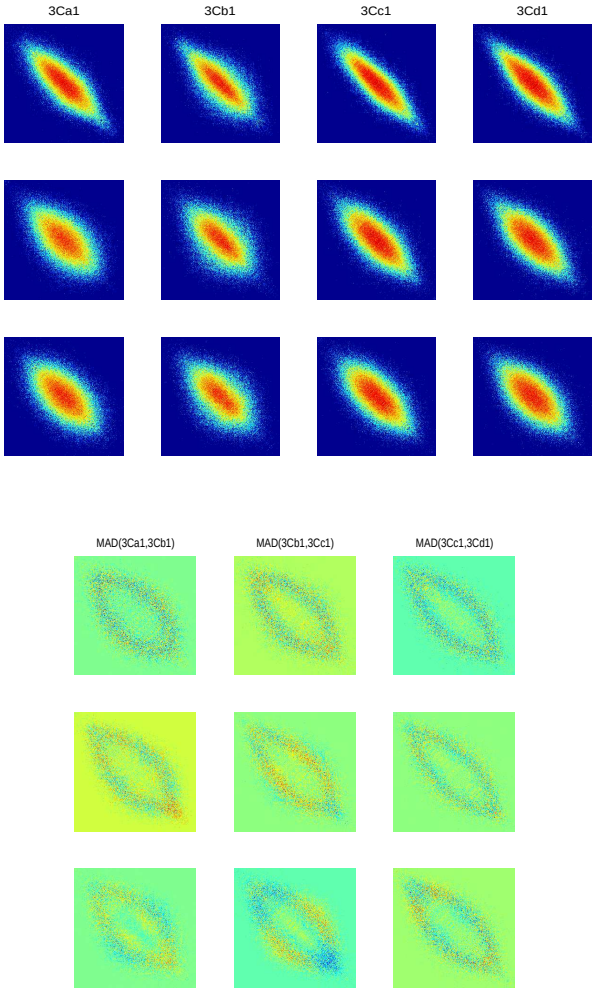

Fig. 14. Co-occurrence matrixes and M.A.D. Components for the case $(3, C)$. The upper part shows the co-occurrence matrixes of the lesion region of selected illumination-corrected images of (Patient 3, Lesion C); from top to bottom, the rows correspond to the red, green and blue band respectively. The lower part shows the MAD components of pairs of consecutive co-occurrence matrixes; from top to bottom, the row number is associated with the MAD component number.

Table 9. Correlation values between the Color Bands and the respective first MAD component for the images of previous Figures

LESION	t_1	t_2	$RED(t_1)$	$GREEN(t_1)$	$BLUE(t_1)$	$RED(t_2)$	$GREEN(t_2)$	$BLUE(t_2)$
1A	a1	b1	-0.043395	-0.281037	0.368620	0.076882	0.296416	-0.397385
1A	b1	c1	0.157975	0.259383	-0.401074	-0.009873	-0.281179	0.280133
1A	c1	d1	0.092474	-0.275296	0.272046	0.360614	-0.083418	-0.280742
1B	a1	b1	0.305761	-0.230549	0.054734	-0.129127	-0.198322	0.343047
1B	b1	c1	0.088509	-0.316239	0.258445	0.320800	-0.068653	-0.275978
1B	c1	d1	0.312352	-0.252936	0.015724	0.163600	-0.290688	0.204880
1C	a1	b1	0.001901	-0.378092	0.510217	-0.069119	0.390545	-0.540887
1C	b1	c1	-0.009486	-0.449951	0.490224	0.001886	0.456618	-0.472794
2A	a1	b1	-0.043036	0.239584	-0.185652	0.216014	-0.191849	0.097690
2A	b1	c1	0.324745	-0.083721	-0.018579	-0.001702	0.211669	-0.210786
2A	c1	d1	0.042016	-0.227695	0.187835	0.266919	-0.140662	0.097644
2B	a1	b1	-0.007383	0.543504	-0.394928	0.019575	0.638896	-0.266538
2B	b1	c1	0.001548	0.637515	-0.242365	-0.047060	-0.669888	0.171656
2B	c1	d1	-0.028495	0.500740	-0.460677	-0.056241	-0.664664	0.193865
2C	a1	b1	-0.015721	-0.194092	0.227168	0.194830	0.101938	-0.189855
2C	b1	c1	0.038893	0.194974	-0.199133	0.048887	0.194801	-0.246159
2C	c1	d1	0.071718	0.195087	-0.221466	0.048802	-0.219207	0.138725
3A	a1	b1	0.083018	-0.214939	0.163499	0.117317	-0.231709	0.145831
3A	b1	c1	0.087001	-0.224819	0.167746	0.143994	-0.213472	0.115006
3A	c1	d1	0.100927	-0.222693	0.149637	-0.087361	0.226875	-0.149954
3B	a1	b1	0.029576	-0.227130	0.222873	-0.001799	0.225008	-0.224343
3B	b1	c1	-0.023228	0.256221	-0.183855	-0.011463	-0.186459	0.174127
3B	c1	d1	0.004763	-0.193600	0.189768	0.011727	0.192159	-0.204803
3C	a1	b1	0.095635	0.177159	-0.248092	-0.110164	0.262144	-0.176593
3C	b1	c1	0.062883	-0.255678	0.199650	0.105009	-0.224865	0.158335
3C	c1	d1	0.073072	-0.232236	0.174764	0.133484	-0.244558	0.131380

References

1. M. Augusteijn and L. Clemens. A performance evaluation of texture measures for image classification and segmentation using the cascade-correlation architecture. *IEEE International Conference on Neural Networks, IEEE World Congress on Computational Intelligence*, 7:4300–4305, 1994.
2. J. Carstensen. *Description and Simulation of visual texture.* PhD thesis, I.M.S.O.R., Technical University of Denmark, Lyngby, April 1992.
3. R. Haralick. Statistical and structural approaches to texture. *Proceedings of the IEEE*, 67(5):786–804, May 1979.
4. K. Hilger. *Exploratory Analysis of Multivariate Data.* Ph.d. thesis, Informatics and Mathematical Modelling. Technical University of Denmark., Kgs. Lyngby, November 2001.
5. R. Larsen. Maf and other transformations applied to remote sensing. Master's thesis, Institute for Mathematical stastistics and Operations Research (IMSOR), Technical University of Denmark, DTU, 1991. pp. xii+130+205.
6. J. Lira and L. Frulla. An automated region growing algorithm for segmentation of texture regions in sar images. *International Journal of Remote Sensing*, 19(18):3595–3606, 1998.
7. J. Lira and G. Maletti. A supervised classifier for multispectral and textured images based on an automated region growing algorithm. *European Space Agency Publications*, SP-434:153–158, 1998.
8. J. Liu, K. Bowyer, D. Goldgof, and S. Sarkar. A comparative study of texture measures for human skin treatment. *International Conference on Information, Communications and Signal Processing*, 1:170–174, September 1997. ICICS'97.
9. G. Maletti and B. Ersbøll. A hierarchical classification scheme of psoriasis images. Technical Report 6, Department of Informatics and Mathematical Modelling. Technical University of Denmark., Kgs. Lyngby. Denmark., March 2003.
10. G. Maletti and B. Ersbøll. Illumination correction in psoriasis lesions images. Technical Report 7, Department of Informatics and Mathematical Modelling. Technical University of Denmark., Kgs. Lyngby. Denmark., March 2003.
11. A. Nielsen. *Analysis of Regularly and Irregularly sampled spatial, multivariate, and muti-temporal data.* PhD thesis, Institute of Mathematical Modelling. Technical University of Denmark., Kgs. Lyngby. Denmark, October 1994. No. 6.
12. A. Nielsen, K. Conradsen, and J. Simpson. Multivariate alteration detection (m.a.d.) and m.a.f. postprocessing in multispectral, bitemporal image data: New approaches to change detection studies. *Remote Sens. Environ.*, 64:1–19, 1998.
13. T. Ojala, M. Peitikäinen, and D. Harwood. A comparative study of textre measures with classification based on feature distributions. *Pattern Recognition*, 29(1):51–59, 1996.
14. S. Peckinpaugh. An improved method for computing gray-level coocurrence matrix based texture measures. *Graphical Models and Image Processing*, 53(6):574–580, November 1991.
15. L. Wang. Vector choice in the texture spectrum approach. *International Journal of Remote Sensing*, 15(18):3823–3829, 1994.
16. L. Wang and D. He. Texture classification using texture spectrum. *Pattern Recognition*, 23(8):905–910, 1990.
17. J. Weszka, Ch. Dyer, and A. Rosenfeld. A comparative study of texture measures for terrain classification. *IEEE Transactions on Systems, Man, and Cybernetics*, SMC-6(4):269–285, April 1976.